Microgrid sizing with combined evolutionary algorithm and MILP unit commitment

Bei Li[a,*], Robin Roche[a], Abdellatif Miraoui[b]

[a] *FEMTO-ST, UMR CNRS 6174, and FCLAB, FR CNRS 3539, Université Bourgogne Franche-Comté, Belfort / UTBM, 90000,France*
[b] *Université Bourgogne Franche-Comté / UTBM, Belfort / UTBM, 90000,France*

Abstract

Microgrids are small scale power systems with local resources for generation, consumption and storage, that can operate connected to the main grid or islanded. In such systems, optimal sizing of components is necessary to ensure secure and reliable energy supply to loads at the least cost. Sizing results are however dependent on the energy management strategy used for operating the system, especially when components with different dynamics are considered. Results are also impacted by uncertainty on load as well as renewable generation. In this paper, we propose a combined sizing and energy management methodology, formulated as a leader-follower problem. The leader problem focuses on sizing and aims at selecting the optimal size for the microgrid components. It is solved using a genetic algorithm. The follower problem, i.e., the energy management issue, is formulated as a unit commitment problem and is solved with a mixed integer linear program. Uncertainties are considered using a form of robust optimization method. Several scenarios are modeled and compared in simulations to show the effectiveness of the proposed method, especially with respect to a simple rule-based strategy.

Keywords: energy management, evolutionary algorithm, microgrid, sizing, unit commitment.

Nomenclature

Acronyms

BSS	battery storage systems
EA	evolutionary algorithms
EMS	energy management systems
ESS	energy storage system
FC	fuel cell
GA	genetic algorithm
HSS	hydrogen storage systems
LOH	level-of-hydrogen
LPSP	loss of power supply probability
MILP	mixed integer linear programming
PV	photovoltaic panels
RBS	rule-based strategies
RES	renewable energy sources
SOC	state-of-charge
UC	unit commitment
WT	wind turbines

Symbols

α	penalty value for load shedding
β	penalty value for curtailed PV output
Δt	sampling time
η_{bat}	BSS charging efficiency
η_{PV}	PV panels efficiency
$\widetilde{P_{load}(t)}$	actual load in time t
$\widetilde{P_{PV}(t)}$	actual output of PV in time t
$B^{ch}_{cost}(t)$	BSS charging cost in time t
$B^{dich}_{cost}(t)$	BSS discharging cost in time t
C^{inv}	investment cost of components
C^{mnt}	annual maintenance costs of components
C_T	PV temperature coefficient
C_{cap}	capital cost of microgrid
C_{mnt}	annual maintenance cost of microgrid
C_{op}	operation cost
C^{inv}_{bat}	investment cost for the BSS
C^{inv}_{ele}	investment cost of the electrolyzer

*Corresponding author.
Email addresses: bei.li@utbm.fr (Bei Li), robin.roche@utbm.fr (Robin Roche), abdellatif.miraoui@utbm.fr (Abdellatif Miraoui)

$C_{ele}^{o\&m}$ operation and maintenance costs of the electrolyzer

C_{ele}^{start} startup cost of the electrolyzer

C_{fc}^{inv} investment cost of the FC

$C_{fc}^{o\&m}$ operation and maintenance costs of the FC

$C_{fc}^{o\&m}$ startup cost of the FC

CRF capital recovery factor

E_{OC} open-circuit voltage of one FC cell

Er_{load} error bound of load

Er_{PV} error bound of PV output

F Faraday constant

$F(.)$ total cost function

G_A global solar radiation

$H_{cost}^{ele}(t)$ utilization cost of the electrolyzer in time t

$H_{cost}^{fc}(t)$ utilization cost of the FC in time t

$I_{el}(t)$ current of the electrolyzer in time t

$I_{el}(t)/A_{el}$ current density of the electrolyzer

$i_{fc}(t)$ current density in one FC cell in time t

$N_{bat,cyc}$ number of cycles of the BSS

$N_{bat,hr}^{ele}$ operation hours of the electrolyzer over its lifetime

$N_{bat,hr}^{fc}$ operation hours of the FC over its lifetime

N_{el} number of electrolyzer cells

N_{fc} number of FC cells

n_{inv} expected life span of the microgrid

$P_{load}(t)$ forecasted load in time t

$P_{PV}(t)$ output power of PV panels in time t

P_{STC} PV array rated power

r real interest rate

T working temperature of the electrolyzer

T_C temperature of panels

T_{hor} time horizon

$V_{el}(t)$ voltage of the electrolyzer in time t

$V_{fc}(t)$ voltage of the FC in time t

V_{rev} reverse voltage of the electrolyzer

Variables

$\Delta\delta_{ele}$ status of the electrolyzer (starting or not)

$\Delta\delta_{fc}$ status of the FC (starting or not)

$\delta_{ele}(t)$ state (on or off) of the electrolyzer

$\delta_{fc}(t)$ state (on or off) of the FC

$\dot{n}_{el}^{H_2}(t)$ production rate of hydrogen of the electrolyzer in time t

$\dot{n}_{fc}^{H_2}(t)$ consumption rate of hydrogen of the FC in time t

C_{bat} capacity of the BSS

$LOH(t)$ state of hydrogen tanks in time t

N_{PV} number of PV panels

$P_{ch}(t)$ BSS charging power in time t

$P_{curt}(t)$ curtailed PV output in time t

$P_{disch}(t)$ BSS discharging power in time t

$P_{el}(t)$ input power of the electrolyzer in time t

$P_{el}^{\max}$ maximum input power of electrolyzer

$P_{fc}(t)$ output power of th FC in time t

$P_{fc}^{\max}$ maximum output power of fuel cell

$P_j(t)$ output power of unit j in time t

$P_{LS}(t)$ shed load in time t

$SOC(t)$ state of BSS in time t

$V_{H_2}^{\max}$ maximum volume of hydrogen tanks

$Z_j(t)$ actual output power of unit j in time t

1. Introduction

In order to limit global warming and reduce fossil fuel consumption, renewable energy sources (RES) such as photovoltaic panels (PV) and wind turbines (WT) are more and more commonly used to generate electricity. The integration of such intermittent sources is a challenge for grid operators, as the balance between generation and demand must be met in real-time. This is especially a concern for small power systems such as microgrids, that can operate islanded, i.e., not connected to the main grid. Microgrids typically include distributed generation and storage [1, 2], and are increasingly found in remote areas [3, 4] or where power system resilience is a crucial concern [5, 6].

To enable RES integration, energy storage systems are considered as a key solution, as they enable storing excess generation for later use [7]. Battery storage systems (BSS) are typically used for short-term storage [8], but seem inappropriate for long-term storage due to their low energy density and non-negligible self-discharge rate [9]. Hydrogen storage systems

(HSS), on the other hand, are used for long-term storage, such as seasonal storage. HSS combine an electrolyzer to produce hydrogen from electricity, an hydrogen storage tank and a fuel cell (FC) to produce electricity from hydrogen. [10] discusses FC systems, while [11] researches about the PV/FC hybrid systems. In [12], a Matlab/Simulink model is built to simulate such a PV/FC hybrid energy system. [13] also builds a simulation model of another PV/FC/ultacapacitors stand-alone microgrid.

In this work, we focus on the optimal sizing of microgrids where PV panels are used as the primary energy source, and BSS and HSS are used as storage units (Fig. 2). Finding the optimal size for each of these components, i.e., finding the capacity or rated power for each component that ensures adequate supply at minimum cost, is a challenge because the sizing result is affected not only by the architecture of the system, but also by the adopted energy management strategy [14]. Depending on how components such as storage units are used, the necessary capacity may change significantly, which in turn impacts the size of other components as well as overall costs. Another aspect to consider is the impact of uncertainty on PV output and load. Forecasting errors change the input data profiles and lead to suboptimal scheduling results, which in turn influences sizing results. To address these challenges, this paper presents a leader-follower co-optimization method to size islanded microgrids, which also considers uncertainty on input data.

The optimal sizing problem is a non-convex and non-linear combinatorial optimization problem [15], and for the solution of this problem, various optimization methods have been presented in [16]. In [17], authors review 68 computer tools which can be used for analyzing RES integration, but the results show that there is no tool that can address all aspects of hybrid microgrid system. As the part of artificial intelligence, evolutionary algorithms (EA) are optimization algorithm which can be used to solve combinatorial and nonlinear optimization problems. For example, [18, 15] compare several EA for the optimal sizing of a hybrid system, where the objective function is the total annual cost. Other papers use various metaheuristics, [19] uses ant colony optimization (ACO) to get size values of PV/wind hybrid system. In [20], artificial bee swarm optimization (ABSO) used to solve the sizing problem of PV/WT/FC hybrid system considering loss of power supply probability (LPSP). Simulated annealing and tabu search (TS) are used in [3]. [21] studies the performance of different particle swarm optimization (PSO) algorithm variants to determine the size results of hybrid (PV/wind/Batt) system.

In most of these papers, a simple control strategy is selected: when there is surplus power, the excess energy is stored in the ESS, and when there is a shortage of power, the ESS discharges, or controllable generators (diesel gensets or FC) are turned on. Economic criteria are not considered in most cases. Some papers use more advanced strategies based on rules (rule-based strategies (RBS)) to control energy flows. Various algorithms are used, such as a multi-objective genetic algorithm (GA) [22], a hybrid GA [23], or an improved bat algorithm [24]. However, the limits of RBS are quickly reached when more than a few components are included in the system, as the number of required rules significantly increases. Moreover, these strategies cannot provide optimal results regarding how the state-of-charge of storage units is controlled over time. More advanced energy management systems (EMS), that primarily focus on economic dispatch with EA, are also presented in the literature. [25] presents a decentralized energy management strategy based on multi-agent systems and fuzzy cognitive Maps. In [26], authors propose a non-cooperative game theory-based EMS. [27] proposes a bi-level optimization energy management approach of multiple microgrids. Economic dispatch is solved in each microgrid, and then a secondary-level optimization is used to seek the minimum operation cost for the set of microgrids. Multiperiod ABCO [28], multi-layer ACO [29], multi-period gravitational search algorithm [30], and multi-period imperialist competition algorithm [31] are also used for economic dispatch applications. [32] presents an operational architecture for Real Time Operation (RTO) of an islanded microgrid. A limit of economic dispatch approaches for EMS is that set points are determined only based on current conditions, but future conditions are not considered.

An improved method for energy management, that can take into account multiple objectives and constraints, is thus required. Model-predictive control (MPC) offers a solution, and is commonly used in power systems in the form of unit commitment (UC). UC enables scheduling the use of multiple generation units over a given time horizon [33], for example over a day. It can also be extended to consider storage units and other devices. For example, in [9], the authors present a UC optimization method to economically schedule BSS and HSS. [34] studies the thermal power plant UC problem integrated with a large scale ESS. In [35], an integrated framework for a stand-alone microgrid with objectives of increasing stability and reliability and reducing costs is described. The UC method is used to determine generators outputs for the next day. [36] presents a two-stage planning and design method for microgrids. GA is used to solve the optimal design problem and a mixed integer linear programming (MILP) algorithm enables determining the optimal operation strategy.In [37], a mixed integer nonlinear programming (MINLP) approach for day-ahead scheduling a combined heat and power plant is proposed. Another MINLP-based EMS algorithm is presented in [38]. [39] describes an approach for security-constrained UC with integrated ESS and wind turbines. Overall, the above research papers show that the UC method is commonly used and adequate for scheduling the use of microgrid components, including energy storage units. However, contrary to works focusing on sizing that primarily focus on EA, papers on UC mainly use classical non-linear or linear programming techniques (MINLP or MILP) [40, 37].

A UC algorithm does however rely on forecast data to compute schedules. As forecasting errors are inevitable, the scheudling algorithm must consider these errors. In the case studied in this paper, errors on PV output and load impact schedules as well as sizing results. Two main approaches to consider forcasting uncertainty are found in the literature: scenario-based method [41, 42, 43] and robust optimization [44, 45, 46, 47]. [41] presents a stochastic method based on cloud theory to handle uncertainty, and uses a krill herd algorithm to solve the optimization problem. [42] describes a stochastic optimization for microgrid energy and reserve scheduling. Wind and PV generation fluctuations for each hour are represented by 5-interval discrete probability distribution functions. A scenario tree technique is then used to combine different states of wind and PV fluctuations. [43] presents a scenario-based robust energy management method. Taguchis orthogonal array testing method is used to provide possible testing scenarios, and determine the worst-case scenario. At last, the Monte Carlo method is used to verify the robustness of the approach. In [44], uncertainty is quantified in terms of prediction intervals by a non-dominated sorting genetic algorithm (NSGA-II) trained by a neural network. Robust optimization is then used to seek the optimal solution to the problem. [45] uses robust optimization-based scheduling for multiple microgrids considering uncertainty. The problem is transformed to a min-max robust problem, and is then solved using linear duality theory and the Karush-Kuhn-Tucker (KKT) optimality conditions. [47] presents a robust EMS for microgrids. Authors use a fuzzy prediction interval model to obtain the uncertainty boundary of wind output, and then the upper and lower boundaries of wind energy are interpreted as the best and worst-case operating conditions. In the above papers, scenario-based methods usually require generating many scenarios , which can take a lot of time to simulate. On the other hand, robust methods are used to find the worst case, which requires less computation time, although results are more conservative. As a consequence, in this paper, a robust optimization method is selected to find the worst case and best case based on the forecasting error.

The above review of the state-of-the-art has shown that a sizing methodology needs to use an appropriate energy management or scheduling approach, and that MPC-based UC fits these needs. Several papers have considered such combinations of sizing and energy management algorithms. For example, [48] presents a co-optimization method to size stand-alone microgrids with two GA: one for the sizing, and another one for the scheduling. In [49], authors present a co-optimization method for microgrid planning in electrical power systems. The leader problem optimizes the planning decisions for the microgrids and the main grid, and, with the proposed plan, the short-term and economic operation subproblems are solved to check whether constraints are met or not. In [50], authors also present a microgrid planning model. The problem is decomposed into an investment master problem and an operation subproblem. The two problems are linked via the benders decomposition method. Finally, in [51], the authors present a bi-level program for the sizing of islanded microgrids with an integrated compressed air energy storage (CAES). The upper level problem is solved using GA, and the lower level problem is solved using the MILP technique.

This paper introduces a general method to size a stand-alone microgrid (PV-BSS-HSS) considering technical and economic criteria, with a combination of EA and UC optimization. Compared to existing literature, contributions include:

1. A bi-level optimization method to perform microgrid sizing. A genetic algorithm is used to compute the sizing of the components to minimize the total annual cost (capital, maintenance and operation) of the system. Each candidate solution (set of components sizes) is evaluated with a MILP UC algorithm. The design bi-level optimization framework is shown in Fig. 1.
2. The used UC optimization is used to control energy flows considers technical and economic criteria, such as the operation costs of the components, the startup costs of the fuel cell and the electrolyzer, the state-of-charge (SOC) of the BSS, the level-of-hydrogen (LOH) of hydrogen tanks. In addition to these, the load shedding and PV power curtailments resulting from sizing values are determined and used to evaluate candidate solutions.
3. A 1-hour resolution rolling-horizon simulation is used to verify the validity of the obtained sizing solutions, and to adjust the sizing values if required, especially as the sizing algorithm input data uses a 1-week resolution to improve computation speed.
4. Uncertainty on PV generation and load is taken into account using a robust method. Sizing results are adjusted depending on forecasting errors.
5. The impact of different initial states for SOC and LOH and different penalty values for load shedding and power curtailments is assessed to determine the sensitivity of results with respect to these parameters.
6. Finally, results are compared with a rule-based strategy commonly used in the literature, in order to further evaluate the performance of the algorithm.

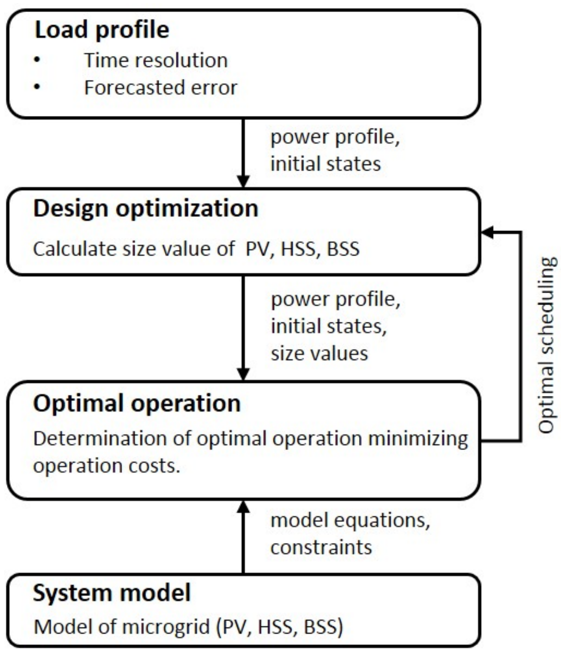

Figure 1: Bi-level optimization framework.

The rest of this paper is structured as follows. Section 2 introduces the system model. Section 3 describes the UC strategy and Section 4 the EA-based sizing problem formulation. Finally, Section 5 presents the simulation results while Section 6 concludes the paper.

2. System model

A stand-alone microgrid with four main components is considered (Fig. 2): PV panels, a BSS, an HSS (with an electrolyzer, hydrogen tanks and a fuel cell), and a load corresponding to a building. Static converters are not modeled, as their impact is negligible on sizing results.

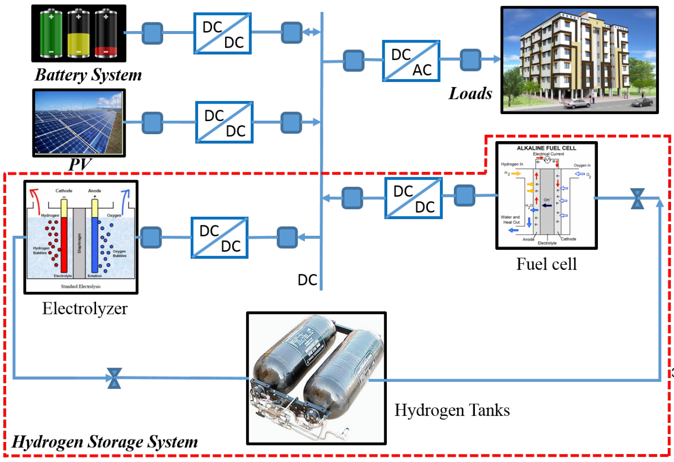

Figure 2: Microgrid architecture.

2.1. PV panels

The output of the PV panels is calculated using [52, 11]:

$$P_{PV}(t) = N_{PV} \cdot \eta_{PV} \cdot P_{STC} \cdot \frac{G_A(t)}{G_{STC}} \cdot (1 + (T_C(t) - T_{STC}) \cdot C_T) \quad (1)$$

where N_{PV} is the number of panels, η_{PV} is the panels efficiency, P_{STC} is the PV array rated power in W_p under standard test conditions (STC), G_A is the global solar radiation received by the panels in kW/m^2, G_{STC} is the solar radiation under STC (1 kW/m^2), T_C is the temperature of the panels, T_{STC} is the STC temperature, and C_T is the PV temperature coefficient.

2.2. Battery

The state of the BSS is represented by its state-of-charge:

$$SOC(t) = SOC(t - \Delta t) + \frac{\eta_b \cdot P_{ch}(t) \cdot \Delta t}{C_{bat}} - \frac{P_{disch}(t) \cdot \Delta t}{C_{bat}} \quad (2)$$

where η_{bat} is the charging efficiency, $P_{ch}(t)$ is charging power, $P_{disch}(t)$ is the discharging power, Δt is the sampling time, and C_{bat} is the capacity of the battery pack.

2.3. Electrolyzer

Electrolyzers are used to produce hydrogen (H_2) from electricity. The characteristic of the electrolyzer can be described as follows [53, 54]:

$$\begin{aligned} V_{el}(t) = \; & N_{el} \cdot V_{rev} + (r_1 + r_2 \cdot T) \cdot \frac{I_{el}(t)}{A_{el}} \\ & + \left(s_1 + s_2 \cdot T + s_3 \cdot T^2\right) \\ & \times log\left(1 + \left(t_1 + \frac{t_2}{T} + \frac{t_3}{T^2}\right) \cdot \frac{I_{el}(t)}{A_{el}}\right) \end{aligned} \quad (3)$$

where $V_{el}(t)$ is the voltage of the electrolyzer, N_{el} is the number of cells, V_{rev} is the reversible cell potential, T is the working temperature (assumed constant), and $I_{el}(t)/A_{el}$ (in A/m^2, with A_{el} the area) is the current density. Variables r_1, r_2, s_1, s_2, s_3, t_1, t_2, t_3 are empirical constant coefficients.

The production rate of hydrogen of the electrolyzer is then given by Faraday's law:

$$\dot{n}_{el}^{H_2}(t) = \eta_F(t) \frac{N_{el}\, I_{el}(t)}{2F} \quad (4)$$

where F is the Faraday constant, and I_{el} is the current in the electrolyzer. η_F is Faraday's efficiency, which provides a relation between the actual production rate of hydrogen and its theoretical value, namely:

$$\eta_F(t) = \frac{(I_{el}(t)/A_{el})^2}{f_1 + (I_{el}(t)/A_{el})^2} f_2 \quad (5)$$

where f_1 and f_2 are empirical coefficients.

Using the above equations, an equation relating $P_{el}(t)$ and $\dot{n}_{el}^{H_2}(t)$ is obtained, in the form of:

$$P_{el}(t) = f(\dot{n}_{el}^{H_2}(t)) \quad (6)$$

where $f(.)$ is a nonlinear function. Due to constraints described in Section 3, this function is linearized, such that:

$$P_{el}(t) = k_{el} \cdot \dot{n}_{el}^{H_2}(t) \quad (7)$$

where k_{el} is a constant. The linearization is done via a linear regression on the curve obtained from (6). The maximum value of P_{el} is noted $P_{el}^{\max}$.

2.4. Fuel cell

Fuel cells consume H_2 and oxygen to produce electricity and water [10, 11, 12, 55]. A simple electrical model is used to describe the characteristic voltage curve of the FC [55]:

$$V_{fc}(t) = (E_{OC} - r_{fc} \cdot i_{fc}(t) - a \cdot ln(i_{fc}(t)) - m \cdot e^{s \cdot i_{fc}(t)}) \cdot N_{fc} \quad (8)$$

where V_{fc} is the voltage of the FC, E_{OC} is the open-circuit voltage of one cell, $i_{fc}(t)$ is the current density in one cell, N_{fc} is the number of cells, and r_{fc}, s, a, and m are empirical coefficients.

The hydrogen consumption of the FC depends on its current and is given by:

$$\dot{n}_{fc}^{H_2}(t) = \frac{N_{fc}\, I_{fc}(t)}{2\, F\, U} \quad (9)$$

where U is the utilization efficiency of hydrogen by the fuel cell.

As for the electrolyzer, the model is linearized to obtain:

$$P_{fc}(t) = k_{fc} \cdot \dot{n}_{fc}^{H_2}(t) \quad (10)$$

where k_{fc} is a constant. The maximum value of P_{fc} is noted $P_{fc}^{\max}$.

2.5. Hydrogen tank

Hydrogen tanks are used to store the hydrogen produced by the electrolyzer. The stored hydrogen is then supplied to the FC to generate electricity. Similarly to the BSS, a quantity named level of hydrogen (LOH) is used to represent the state of the tank:

$$LOH(t) = LOH(t - \Delta t) + \dot{n}_{el}^{H_2}(t) \cdot \Delta t - \dot{n}_{fc}^{H_2}(t) \cdot \Delta t \quad (11)$$

Then, using the ideal gas law ($PV = nRT$), the volume of the tank V_{H_2} can easily be determined.

3. Scheduling strategy

As the results of the sizing process depend on how the different components are used (i.e., what is their output), an appropriate control strategy is required. Contrary to classical components, ESS introduce a temporal link between time steps and scheduling algorithms have to consider this link to ensure that the SOC remains within allowed bounds. This constraint is necessary to ensure that the results of the sizing are adequate, and components oversizing is avoided. As a consequence, it is necessary to predict the evolution of the entire system, including the PV generation which is the primary source of energy for the microgrid.

This paper uses a form of MPC to plan the operation of the system in advance, using forecasts. This MPC strategy is a UC algorithm. Due to the presence of mixed logical and integer variables, the problem is expressed as a MILP problem.

3.1. Cost function

In order to achieve economically efficient operation, the utilization cost of the BSS and the HSS need to be quantified and minimized over a given time horizon [9, 56, 48]. For the BSS, aging is a major concern that limits the lifetime of the device. As a consequence, the investment cost and the degradation of the BSS have to be taken int account in the operation cost. The utilization cost for charge and discharge are then implemented as follows [56]:

$$B_{cost}^{ch}(t) = \frac{C_{bat}^{inv} \cdot P_{ch}(t) \cdot \eta_b}{2 \cdot N_{bat,cyc}} \quad (12)$$

$$B_{cost}^{disch}(t) = \frac{C_{bat}^{inv} \cdot P_{disch}(t)}{2 \cdot N_{bat,cyc}} \quad (13)$$

where C_{bat}^{inv} is the investment cost for the BSS, and $N_{bat,cyc}$ the number of cycles over its lifetime.

For the HSS, the O&M and the startup costs must also be considered. The utilization cost of the electrolyzer and the FC can be computed as follows [56]:

$$H_{cost}^{ele}(t) = \left(\frac{C_{ele}^{inv}}{N_{bat,hr}^{ele}} + C_{ele}^{o\&m} \right) \cdot \delta_{ele}(t) + C_{ele}^{start} \cdot \Delta\delta_{ele}(t) \quad (14)$$

$$H_{cost}^{fc}(t) = \left(\frac{C_{fc}^{inv}}{N_{bat,hr}^{fc}} + C_{fc}^{o\&m} \right) \cdot \delta_{fc}(t) + C_{fc}^{start} \cdot \Delta\delta_{fc}(t) \quad (15)$$

where C_{ele}^{inv} and C_{fc}^{inv} are the investment costs for the electrolyzer and the FC. $C_{ele}^{o\&m}$ and $C_{fc}^{o\&m}$ are the operation and maintenance costs of both components. Similarly, C_{ele}^{start} and C_{fc}^{start} are their startup cost. $N_{bat,hr}$ represents the number of hours of operation of the HSS over its lifetime. $\delta_{ele}(t)$ and $\delta_{fc}(t)$ describe their state (i.e., 1 for on, 0 for off). Finally, $\Delta\delta_i$ represents whether the unit is starting or not, and is defined as:

$$\Delta\delta_i(t) = \max\{\delta_i(t) - \delta_i(t-1), 0\}, i = \{ele, fc\} \quad (16)$$

Based on the previous cost functions, the total operation cost function for the entire microgrid, over a time horizon of T_{hor} steps, can be built:

$$\begin{aligned} C_{\text{op}} = \sum_{t=1}^{T_{hor}} \Big(& B_{cost}^{ch}(t) + B_{cost}^{dis}(t) + H_{cost}^{ele}(t) + H_{cost}^{fc}(t) \\ & + \alpha \cdot P_{LS}(t) + \beta \cdot P_{curt}(t) \Big) \end{aligned} \quad (17)$$

where $P_{LS}(t)$ is the shed load, $P_{curt}(t)$ is the curtailed PV output, and α and β are the corresponding penalty values. Load shedding (LS) and PV curtailment (PVC) are two means of flexibility to ensure a balance between generation and demand. However, their use has to be minimized due to their impact on customer comfort and system efficiency, respectively. The values of penalty coefficients α and β are thus chosen to discourage the use of LS and PVC. A form of demand response could however also be used [57, 58], but is kept for future work.

3.2. Constraints

The operation of the various components is subject to several constraints, as is the islanded operation of the system. In the following equations, $i = \{ele, fc\}$ and $j = \{ele, fc, ch, disch\}$. First, all component outputs have to be between their minimum and maximum values:

$$P_j^{min} \leq P_j(t) \leq P_j^{\max} \quad (18)$$

In order to consider the status of each device (on or off), the above equation becomes:

$$\delta_j(t) \cdot P_j^{min} \leq Z_j(t) = \delta_j(t) \cdot P_j(t) \leq \delta_j(t) \cdot P_j^{\max} \quad (19)$$

Due to linearity constraints, this equation can then in turn be transformed into the following two inequalities:

$$\begin{aligned} Z_j(t) &\leq P_j(t) - (1 - \delta_j(t)) \cdot P_j^{min} \\ Z_j(t) &\geq P_j(t) - (1 - \delta_j(t)) \cdot P_j^{\max} \end{aligned} \quad (20)$$

Another constraint is that the electrolyzer and the FC should not be working at the same time, i.e., the HSS is either charging or discharging:

$$\delta_{ele}(t) + \delta_{fc}(t) \leq 1 \quad (21)$$

A similar constraint is used for the BSS:

$$\delta_{ch}(t) + \delta_{disch}(t) \leq 1 \quad (22)$$

The SOC and LOH constraints also have to be verified:

$$SOC_{min} \leq SOC(t) \leq SOC_{max} \tag{23}$$

$$V_{H_2}^{min} \leq V_{H_2}(t) \leq V_{H_2}^{\max} \tag{24}$$

Then, equation (16) can be rewritten as:

$$\Delta\delta_i(t) = \delta_i(t) \cdot (1 - \delta_i(t-1)), i = \{ele, fc\} \tag{25}$$

From [59], the above nonlinear equation can be transformed into the following linear constraints:

$$-\delta_i(t) + \Delta\delta_i(t) \leq 0 \tag{26}$$

$$-(1 - \delta_i(t-1)) + \Delta\delta_i(t) \leq 0 \tag{27}$$

$$\delta_i(t) + (1 - \delta_i(t-1)) - \Delta\delta_i(t) \leq 1 \tag{28}$$

Finally, as the system is islanded, the balance between generation and demand has to be met at all time steps, so:

$$\begin{aligned} P_{PV}(t) - P_{curt}(t) - (P_{load}(t) - P_{LS}(t)) \\ = Z_{ele}(t) - Z_{fc}(t) + Z_{ch}(t) - Z_{dis}(t) \end{aligned} \tag{29}$$

3.3. Problem formulation

Using the above cost function and constraints, the microgrid UC problem can be summarized as follows, where $\widetilde{S}$ is the set of variables:

$$\min_{\widetilde{S}}\{C_{\text{op}}\} \quad \text{s.t.} \;\; (2),(7),(10),(11),(18)-(29) \tag{30}$$

4. Sizing algorithm

The scheduling strategy presented in the previous section requires several input variables. Some of these variables correspond to the maximum rating or capacity of each component, what are the results of the sizing algorithm. Other inputs are parameters set by the user, such as the initial SOC and LOH values, and the penalty coefficients α and β. The impact of these parameters on results will be discussed in Section 5.

4.1. Leader-follower structure

The sizing problem aims at finding the optimal size of the PV, BSS, electrolyzer and FC components to achieve the most cost-effective solution over a given time period. Let $N_{PV} \in \mathbf{N_{PV}}$, $C_{bat} \in \mathbf{C_{bat}}$, $V_{H_2}^{\max} \in \mathbf{V_{H_2}}$, $P_{el}^{\max} \in \mathbf{P_{el}}$, $P_{fc}^{\max} \in \mathbf{P_{fc}}$. Set $\mathbf{U}$ represent the whole set, namely, $\mathbf{U} = \mathbf{N_{PV}} \cup \mathbf{C_{bat}} \cup \mathbf{V_{H_2}} \cup \mathbf{P_{el}} \cup \mathbf{P_{fc}}$, and $U \in \mathbf{U}$.

The problem can then be formulated as a leader-follower problem [60]. The leader problem (the sizing problem) is as follows:

$$\min_{U \in \mathbf{U}}\{F(\mathbf{U})\} \tag{31}$$

where $F(.)$ is a function representing the total cost of the system over the simulation duration.

The follower problem (the scheduling problem), is defined as:

$$\min_{U^*,\widetilde{S}}\{C_{\text{op}}\} \quad \text{s.t.} \;\; (2),(7),(10),(11),(18)-(29) \tag{32}$$

where U^* is the set of sizing values obtained from the leader.

In other words, the leader first returns a candidate set of values for N_{PV}, C_{bat}, $V_{H_2}^{\max}$, $P_{el}^{\max}$, and $P_{fc}^{\max}$. Then the follower uses these values to calculate the total operation cost using the algorithm described in Section 3. Based on this cost information, the leader adjusts the sizing values until an optimal value that minimizes the overall cost is found.

4.2. Leader problem objective function

To obtain a valid estimate of the actual cost of the system, operation cost is insufficient as capital and maintenance costs must also be considered [15, 48, 18]. In order to convert the initial capital cost to an annual capital cost, the capital recovery factor (CRF) is used [15]:

$$CRF = \frac{r(1+r)^{n_{inv}}}{(1+r)^{n_{inv}} - 1} \tag{33}$$

where r is the real interest rate and n_{inv} is the expected life span of the microgrid.

The total capital cost corresponds to the cost of buying the equipment, given by:

$$\begin{aligned} C_{\text{cap}} = CRF \cdot (N_{PV} \cdot C_{PV}^{inv} + P_{fc}^{\max} \cdot C_{fc}^{inv} + P_{el}^{\max} \cdot C_{ele}^{inv} \\ + V_{H_2} \cdot C_{tank}^{inv} + C_{bat} \cdot C_{bat}^{inv}) \end{aligned} \tag{34}$$

where C^{inv} variables represent the prices of the PV, FC, electrolyzer, hydrogen tanks and battery components.

Similarly, the annual maintenance cost is given by:

$$C_{\text{mnt}} = N_{PV} \cdot C_{PV}^{mnt} + V_{H_2} \cdot C_{tank}^{mnt} + C_{bat} \cdot C_{bat}^{mnt} \tag{35}$$

where C^{mnt} variables represent the annual maintenance costs of the PV, hydrogen tanks and battery components. As the O&M cost of the FC and the electrolyzer are considered in the operation strategy equations (12) to (15), they are not included in the annual cost.

The fitness function of the leader problem is thus the total cost function $F(.)$ given by:

$$F = C_{\text{cap}} + C_{\text{op}} + C_{\text{mnt}} \tag{36}$$

Finally, the overall problem can be formulated as:

$$\begin{aligned} &\min_{U \in \mathbf{U}}\{C_{\text{cap}} + \min_{U^*,\widetilde{S}}\{C_{\text{op}}\} + C_{\text{mnt}}\} \\ &s.t. \;\; (2),(7),(10),(11),(18)-(29) \end{aligned} \tag{37}$$

4.3. Simulation process

In order to obtain the optimal sizing for the system, the MILP-based scheduling algorithm and the EA-based sizing algorithm are combined.

A GA [23, 61] is used to solve the leader problem. GA are based on the natural selection process similar to biological evolution. Operators such as mutations, crossover and selection enable generating candidate solutions. The decision variables of the GA are rounded to the nearest higher value for use in the UC MILP algorithm.

The simulation process is shown in Fig. 3:

1. The population of N candidate solutions for the GA is randomly initialized.
2. Each of these solutions is then used with the follower problem. The UC MILP optimization is run. If the solution is infeasible, a new candidate solution is generated.
3. The GA fitness function value is then computed to determine the total cost of each candidate solution.
4. The process continues until any stopping criterion is met. An adaptive method is selected. Firstly, if the fitness function values for two consecutive steps are the same, then counter Num is incremented. If Num exceeds a given maximum value (here $Num^{max} = 50$), the simulation stops as the fitness function is not improving anymore. The second criterion is on the number of iterations, for which a maximum number (here $Gen^{max} = 200$) is set.

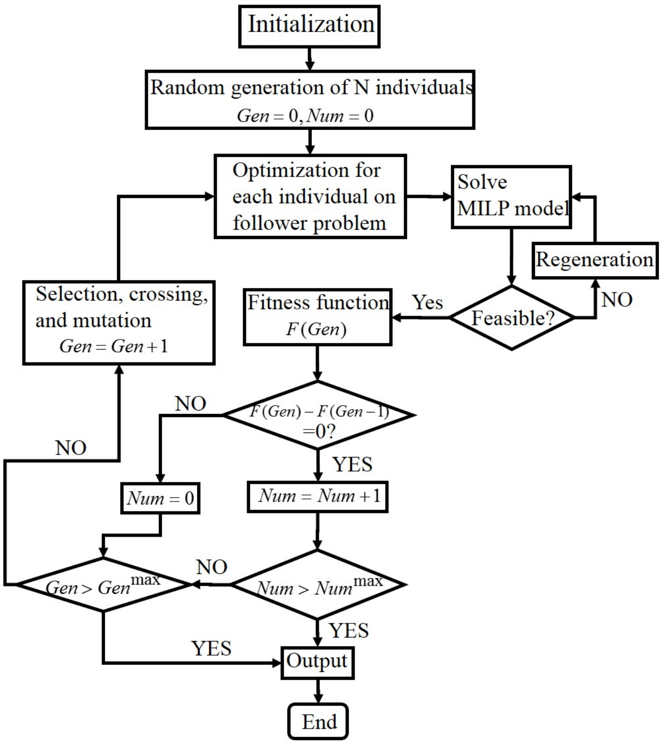

Figure 3: Optimization process outline.

5. Simulation results

In order to validate the sizing methodology, we run several simulation cases.

5.1. Simulation setup

Simulations are performed using Matlab R2014a and Gurobi 6.5.1, running on a desktop computer with an Intel Xeon 3.1 GHz processor, 16 GB RAM, and Microsoft Windows 7. Input data profiles for solar radiation and load (Fig. 4) are obtained and adapted from a research building located on the UTBM campus in Belfort, France. In order to analyze the sensitivity of sizing results to load levels, we use two load profiles. As shown in Fig. 4, load profile 2 is 50% larger than load profile 1. Component parameters used in the simulations are given in Table 1.

In order to keep simulation time to reasonable durations, weekly average data is used for the input data. The approximate duration for each run is then of approximately 30 minutes. Although resolutions of 1 hour or more could be used, simulation durations would increase significantly and could not be performed on a regular computer.

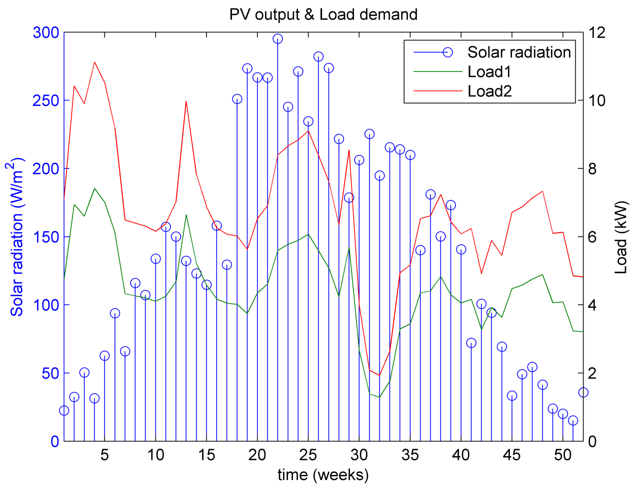

Figure 4: Weekly average solar radiation and load profiles.

5.2. Cases overview

To evaluate the impact of initial conditions and parameters, five cases are compared. Each case assumes different values for SOC_{ini}, LOH_{ini}, α and β, and one of the two load profiles. Case assumptions are summarized in Table 2. Cases 1A and 1B, and Cases 2A and 2B are designed to compare the influence of different initial states for SOC and LOH on the sizing results. Case 2 is also used to analyze the influence of different load levels on the sizing of the HSS and the BSS. Case 3 is designed to analyze the influence of the penalty values (α and β) on sizing results, with values ranging from 10^5 to 10^1. Results are summarized in Table 3.

5.3. Results for Case 1

For Case 1A, the sizing results return 52 PV panels, a 6 kW FC, a 7 kW electrolyzer, tanks with a capacity of 7178 Nm^3, and 189 kWh of batteries, for a total cost of €201,970. Here, unit Nm^3 corresponds to the volume under normal conditions (1 bar, 0°C). Based on the ideal gas law, we can estimate the volume for a higher pressure and temperature. For example, under 700 bar/15°C, the above volume would amount to 10.82 m^3. Convergence results of the GA are shown in Fig. 5, and indicate that 200 generations seem sufficient. Similar convergence results are obtained for other cases.

Fig. 6 shows the scheduling results. The HSS is more frequently used than the BSS, as the HSS is cheaper to use when the power gap between PV output and load demand is large.

Table 1: Component and simulation parameters.

Fuel cell [10, 11, 12, 55, 48]	
A	0.03
r_{fc}	2.45×10^{-4}
m	2.11×10^{-5}
n	0.008
C_{fc}^{inv}	4,000 €/kW
$C_{fc}^{o\&m}$	0.2 €/h
Life cycles	30,000h
P_{fc}^{min}	1kW
Electrolyzer [53, 54, 48]	
r_1	0.0015
r_2	-6.019×10^{-6}
s_1	2.427
s_2	-0.0307
s_3	3.9×10^{-4}
t_1	0.214
t_2	-9.87
t_3	119.1
f_1	150
f_2	0.99
C_{ele}^{inv}	3,200 €/kW
$C_{fc}^{o\&m}$	0.2 €/h
Life cycles	30,000h
P_{ele}^{min}	1kW
Battery [48]	
C_{bat}^{inv}	470 €/kWh
C_{bat}^{mnt}	1 €/kW.year
$N_{bat,cyc}$	2,000
SOC_{min}	0.5
SOC_{max}	0.9
Hydrogen tanks [48]	
C_{tank}^{inv}	150 €/Nm^3
C_{tank}^{mnt}	10 €/Nm^3.year
$V_{H_2}^{min}$	1Nm^3
PV panels[48]	
C_{PV}^{inv}	7,400 €/kW
C_{PV}^{mnt}	6 €/kW.year
CRF [48]	
n_{inv}	20 years
r	0.05

Table 2: Simulation cases assumptions.

Cases	1A	1B	2A	2B	3
SOC_{ini}	0.5	0.9	0.5	0.9	0.5
LOH_{ini}	5000	3000	8000	7000	5000
α	10^5	10^5	10^5	10^5	10^3
β	10^5	10^5	10^5	10^5	10^3
Load profile	1	1	2	2	1

Fig. 7 shows the change in hydrogen level in the tanks. As in winter the PV output is insufficient, the HSS discharges mostly to supply the load, but in summer, PV output is large enough to enable the HSS to recharge and store hydrogen. Due to the large penalty values (10^5) for LS and PVC, these two options are almost not used.

Fig. 7 also shows the SOC profile of the BSS, that is used as an auxiliary storage system to ensure the balance between generation and demand, while avoiding load shedding and PV curtailment.

For Case 1B, the initial SOC is larger and the initial LOH lower. The capacity of the hydrogen tank decreases to 5283 Nm^3, while the battery capacity decreases to 179 kWh. Consequently, the total cost also decreases to € 160,070. The scheduling results for Case 1B are similar to the ones obtained for Case 1A, and are thus not shown. Fig. 8 shows the LOH and SOC levels. As the initial SOC is larger than for 1A, the total required capacity is lower. For the LOH, the profile is almost the same as in Case 1A. For the SOC, in Case 1A, the initial state is the minimum SOC, so the BSS cannot discharge at the beginning, but for Case 1B, the initial state is the maximum SOC and the BSS can then discharge.

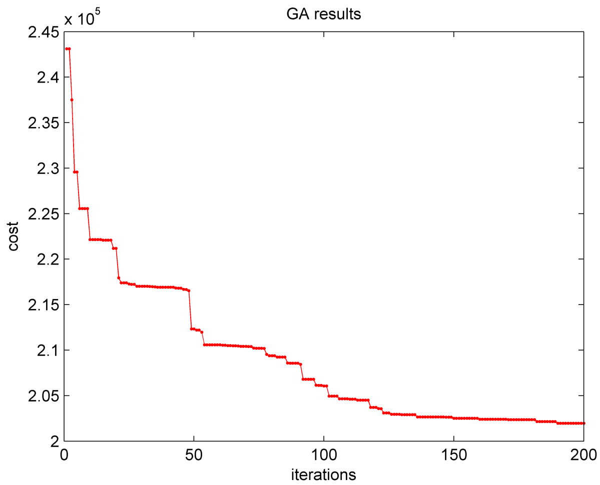

Figure 5: Comparison of the convergence of all three EA for Case 1A.

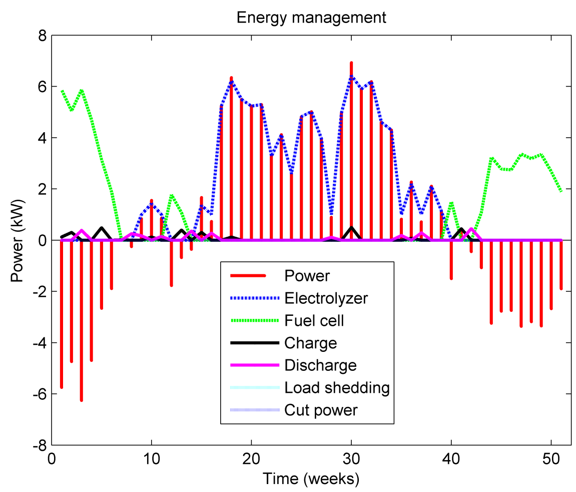

Figure 6: Scheduling results for case 1A. The curve labelled 'Power' corresponds to the PV output minus the load.

Table 3: Sizing results.

Case	Load	SOC_i	LOH_i	Total Cost [€]	C_{op} [€]	C_{cap} [€]	N_{PV}	P_{fc}^{max} [kW]	P_{el}^{max} [kW]	V_{H_2} [N.m^3]	C_{bat} [kWh]
1A	1	0.5	5000	201970	1697.8	127980	52	6	7	7178	189
1B	1	0.9	3000	160070	1663.2	105070	52	6	7	5283	179
2A	2	0.5	8000	219410	1725.1	137210	50	11	6	8000	158
2B	2	0.9	7000	200290	1674.5	128090	54	10	7	7000	190
3	1	0.5	5000	205160	4562.2	125120	52	7	7	7515	2
RBS	1	0.5	5000	276560	151.9	174640	57	7	8	10100	407

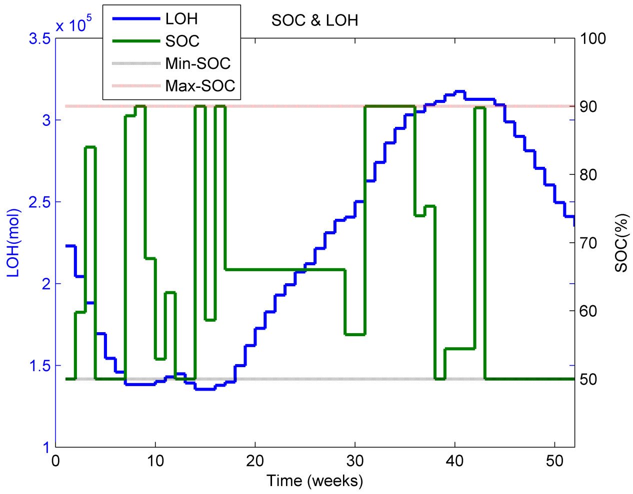

Figure 7: LOH and SOC for Case 1A.

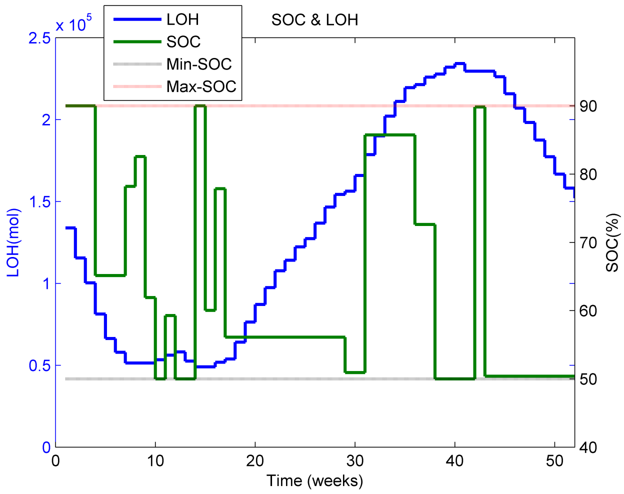

Figure 8: LOH and SOC for Case 1B.

5.4. Results for Case 2

For Cases 2A and 2B, the second load profile with a 50% higher demand is used. For Case 2A, the sizing results return 50 PV panels, a 11 kW FC, a 6 kW electrolyzer, tanks with a capacity of 8000 Nm^3, and 158 kWh of batteries, for a total cost of €219,410. Fig. 9 shows the scheduling results, and Fig. 10 the LOH and SOC profiles. The HSS is sufficient to provide energy to the load, especially at the beginning, so the needed battery capapcity is lower. However, in Case 2B, the HSS is insufficient to meet the load, so more PV panels and battery energy are needed. We can also see that the rating of the FC is larger than in Case 1. As more energy is needed, it becomes cheaper to use the FC than the battery, hence the higher FC rating.

For Case 2B, the sizing results return 54 PV panels, a 10 kW FC, a 7 kW electrolyzer, tanks with a capacity of 7000 Nm^3, and 190 kWh of batteries, for a total cost of €200,290. As the load is higher than that of Case 1, more storage, in the form of BSS and HSS is needed. As the cost of the energy initially contained in the storage units is not accounted for, the algorithm increases the size of the storage units rather than increasing the number of PV panels. The obtained scheduling results are close to the ones shown in Fig. 9. Fig. 11 shows the LOH and SOC profiles. Due to slight differences in the scheduling results, the SOC curve is difference from the one in Case 2A. However, the curves for LOH is similar, as the HSS operates as a longer term storage unit.

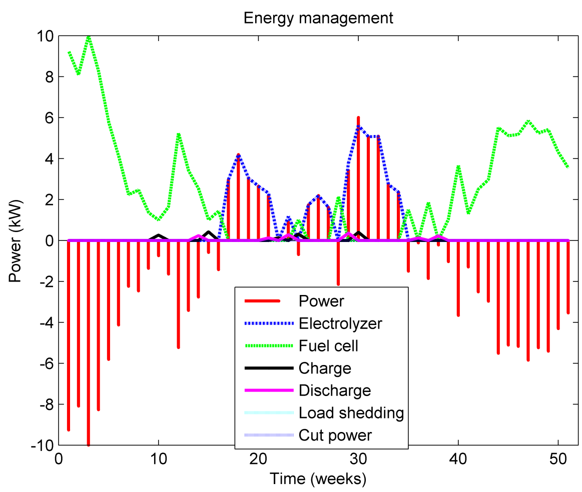

Figure 9: Scheduling results for Case 2A. The curve labelled 'Power' corresponds to the PV output minus the load.

5.5. Results for Case 3

In this case, as the penalty values are lower (10^3 instead of 10^5), more energy is shed or curtailed. As a consequence, the

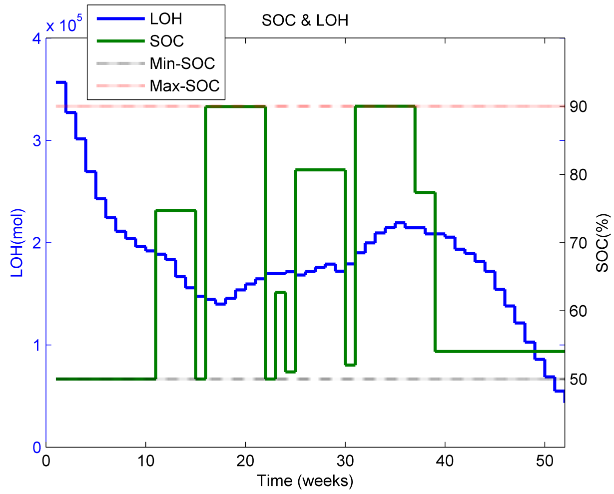

Figure 10: LOH and SOC for Case 2A.

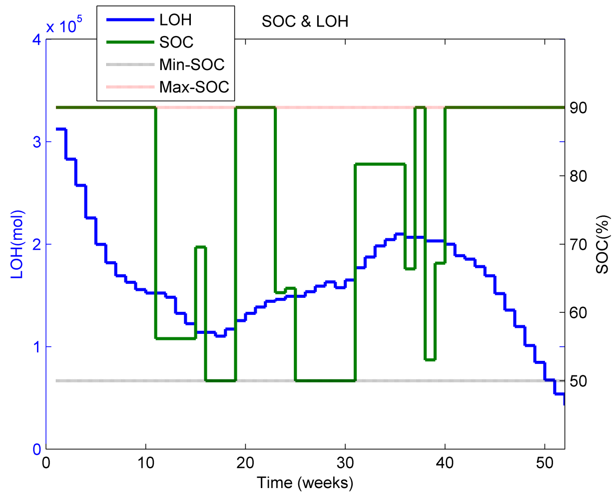

Figure 11: LOH and SOC for Case 2B.

sizing results return 52 PV panels, a 7 kW FC, a 7 kW electrolyzer, tanks with a capacity of 7515 Nm^3, and 2 kWh of batteries, for a total cost of €205,160. Detailed LS, PVC, LOH and SOC profiles are shown in Fig. 15.

The size of the battery is significantly smaller than in other cases. This can be explained by the lower values of the penalties for LS and PVC, which make these two options more competitive compared to using the BSS. In order to futher evaluate the influence of the different penalty values, we simulate different combinations of α and β with Case 1A. The results are shown in Table4 and Figs. 12 and 13, and indicate that the smaller the values of α and β, the larger the magnitude of LS and PVC, respectively.

Scheduling results are shown in Fig. 14, where we observe that limited LS and PVC occur, although for Cases 1 and 2 the BSS was used to supply the load (due to its cheaper cost). As expected, the algorithm choses the most economical way to operate the system.

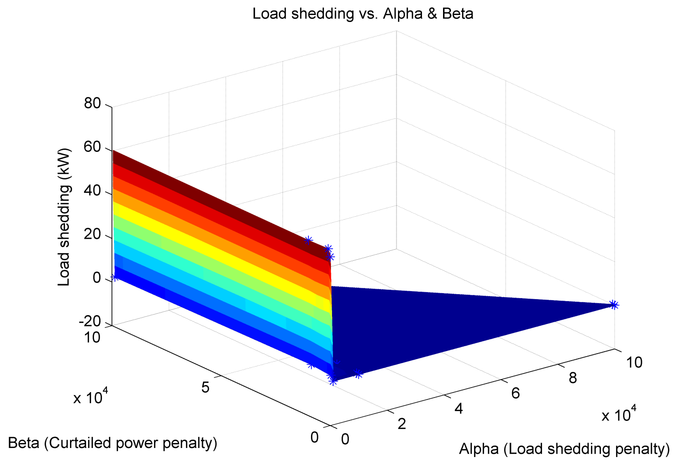

Figure 12: Load shedding vs. α & β.

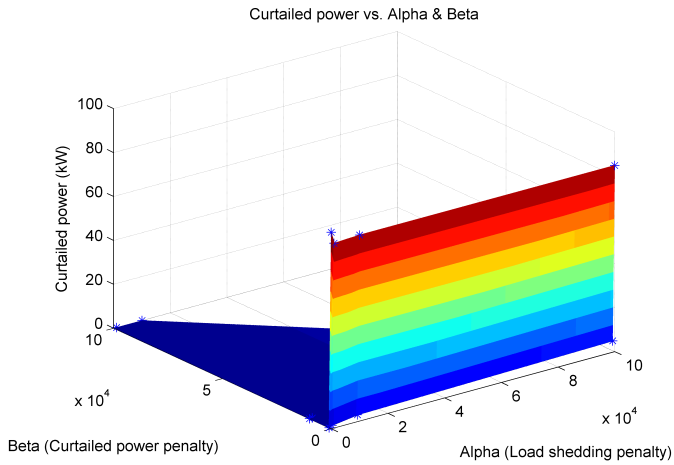

Figure 13: Curtailed power vs. α & β.

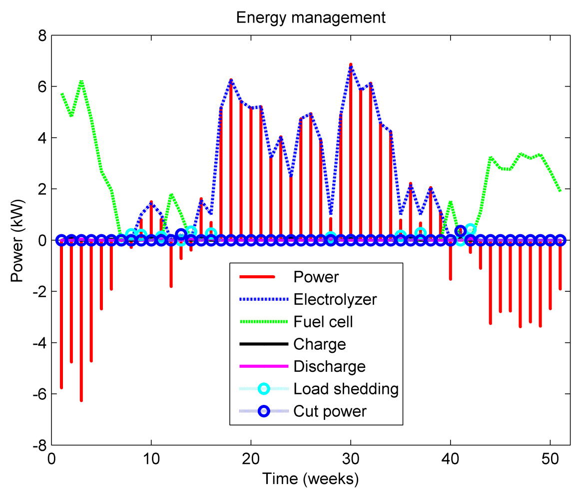

Figure 14: Scheduling results for Case 3. The curve labelled 'Power' corresponds to the PV output minus the load

Table 4: Sizing results with different penalty values for Case 1A.

Case 3	$\sum_{t=1}^{T_{hor}} P_{LS}(t)$ [kW]	$\sum_{t=1}^{T_{hor}} P_{curt}(t)$ [kW]	N_{PV}	$P_{fc}^{\max}$ [kW]	$P_{el}^{\max}$ [kW]	V_{H_2} [N.m^3]	C_{bat} [kWh]
$\alpha = 10^5, \beta = 10^3$	0	4.4576	51	7	7	6823	58
$\alpha = 10^5, \beta = 10^1$	0	84.8847	50	7	1	5026	2
$\alpha = 10^4, \beta = 10^1$	0	84.7377	50	7	2	5543	2
$\alpha = 10^4, \beta = 10^3$	0.0839	2.4054	55	7	8	8341	2
$\alpha = 10^4, \beta = 10^4$	0.0352	0	52	6	7	7601	170
$\alpha = 10^4, \beta = 10^5$	0.1297	0	59	7	8	11123	113
$\alpha = 10^3, \beta = 10^1$	0	84.1643	50	7	2	7015	2
$\alpha = 10^3, \beta = 10^3$	2.209	0.7691	52	7	7	7515	2
$\alpha = 10^3, \beta = 10^4$	3.0844	0	52	7	8	10978	11
$\alpha = 10^3, \beta = 10^5$	1.9553	0	54	7	8	8315	38
$\alpha = 10^1, \beta = 10^1$	57.3662	89.4729	50	2	2	5793	2
$\alpha = 10^1, \beta = 10^3$	60.5996	0	50	2	7	9110	1
$\alpha = 10^1, \beta = 10^4$	60.3302	0	50	2	7	9023	2
$\alpha = 10^1, \beta = 10^5$	60.5804	0	50	2	7	9157	2

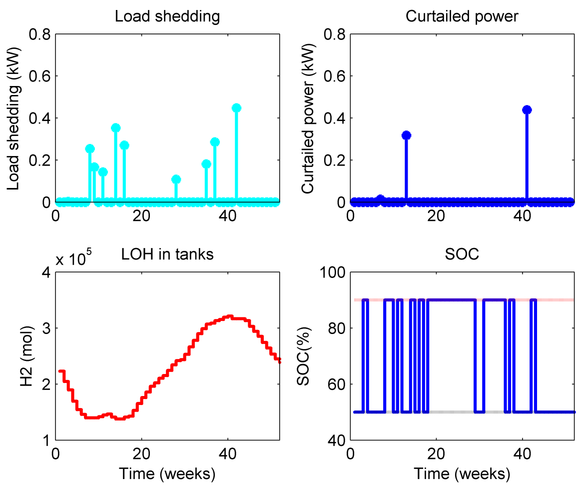

Figure 15: Shed and curtailed power, LOH and SOC profiles for Case 3.

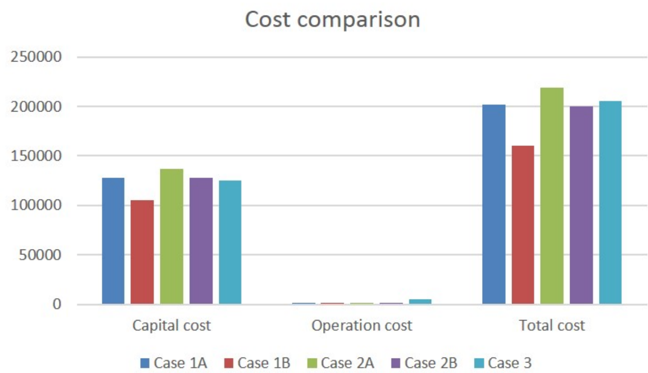

Figure 16: Comparison of costs for all cases.

5.6. Discussion of Cases 1 to 3

From the summary of results shown in Table 3, it can be observed that the sizing results and the total cost are impacted by the use of different input data and initial states. A comparison of the breakdown of costs for all cases is shown in Fig. 16. Results indicate that the capital costs are the highest, while O&M costs remain relatively small. As the only primary energy source is PV, these results are not surprising. The initial energy contained in the BSS and the HSS is however not considered. Case 3 has the largest O&M cost, due to the penalty values combined to LS and PVC. For Case 2A, more fuel cell and hydrogen tanks are needed, which results in the largest capital and total cost.

Simulations also show that the HSS is more appropriate for long term (seasonal) storage, as expected. This is especially valid as FC and electrolyzers have limited dynamics, and require BSS or other fast dynamics storage units to complement them and act as an auxiliary unit. On the other hand, because the discharge and charge power of the HSS are separate, the degration of the HSS will be slower than for the BSS.

Regarding LS and PVC penalty values, results have shown that values in the range of value $[10^3, 10^5]$ are reasonable and enable limiting the use of LS and PVC only to necessary cases. Values larger than 10^5 result in no LS or PVC at all, which can be problematic are they can be seen as flexibility means of last resort.

5.7. Comparison with a rule-based operation strategy

In order to compare the obtained results with a simpler, reference case, we implement a rule-based operation strategy (RBS) [13, 62]. The outline of the algorithm is shown in Fig.17. The principle is to use the HSS first, and if it is unavailable, to use the BSS. It should be noted that the algorithm does not try to maintain the SOC or LOH level for future use, contrary to the proposed algorithm. Case 1A is run again with the RBS. Results, also given in Table 3, show that because using HSS is cheaper, the operation cost is low, but then more BSS capacity is required to ensure power balance. As a consequence, the total capital cost is the largest of all cases.

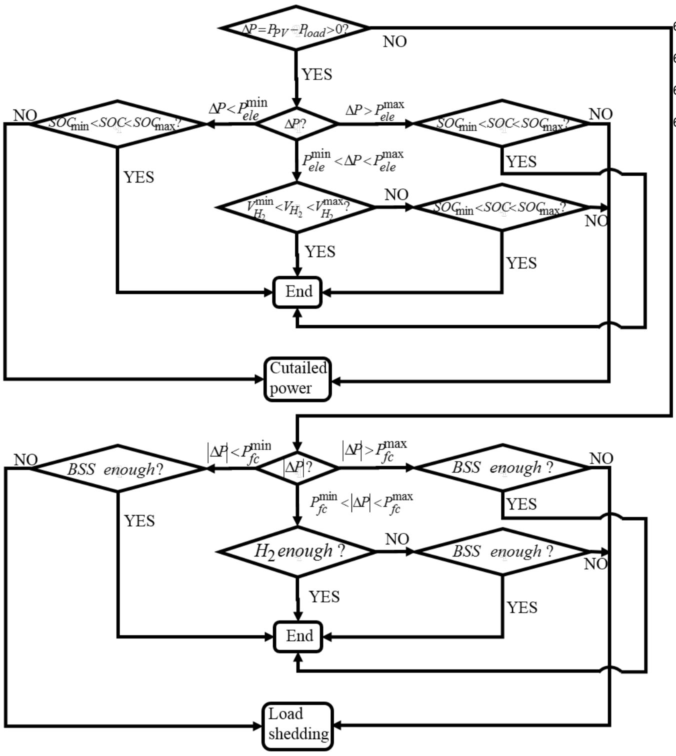

Figure 17: Rule-based strategy algorithm.

5.8. *Influence of time resolution*

In the above simulation, one-week average data is used. A better time resolution (for example, one day or one hour) may provide more accurate results; however, this would also significantly increase computation time to several days or more. In order to check the validity of the obtained results with more precise input data, a rolling-horizon scheduling simulation with a 1-hour time resolution is conducted. This resolution is selected as it is the maximum resolution available for the input data. In summary, the algorithm runs a scheduling task with 1-hour data over 1 day, and repeats this every day for a year.

Results are shown in Figs. 18 (SOC, LOH, LS and PVC) and 19 (scheduling results from 2000 hour to 2300 hour). From these curves, it can be observed that large LS and PVC occur during some periods of the year. As LS and PVC use are supposed to remain rare, this means that the sizing results are insufficient. A reason for this result is that the average data reflects the average load in the system, but does not consider peak load situations. A similar reasoning may be used for PV generation.

In order to adjust sizing results, the difference between PV output and load demand is computed and shown in Fig. 20. Then we adopt the maximum shortage value (i.e., the minimum value in Fig. 20) as the capacity of fuel cell, and the maximum surplus value (i.e., the maximum value in Fig. 20) as the capacity of electrolyzer. And sizing value of the HSS are adjusted, so that $P_{fc}^{max} = 13$, $P_{ele}^{max} = 37$.

After this adjustment, the rolling-horizon simulation is run again. Fig. 21 shows the resulting SOC, LOH, LS and PVC, and Fig. 22 shows the scheduling results from 2000 hour to 2300 hour with the new sizing values. After adjusting the sizing value based on the peak load demand, no LS or PVC occur. And with the adjusted sizing values, we run MILP scheduling for case1A, and total cost is €212160, operation cost C_{op} is €1788.7, and capacital cost C_{cap} is €138080.

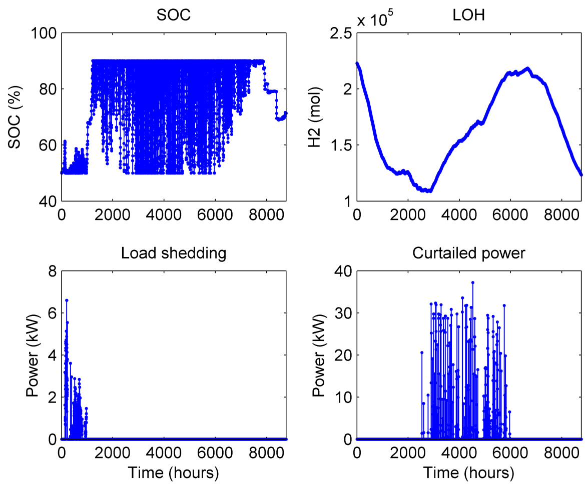

Figure 18: One-hour one-day rolling horizon scheduling simulation.

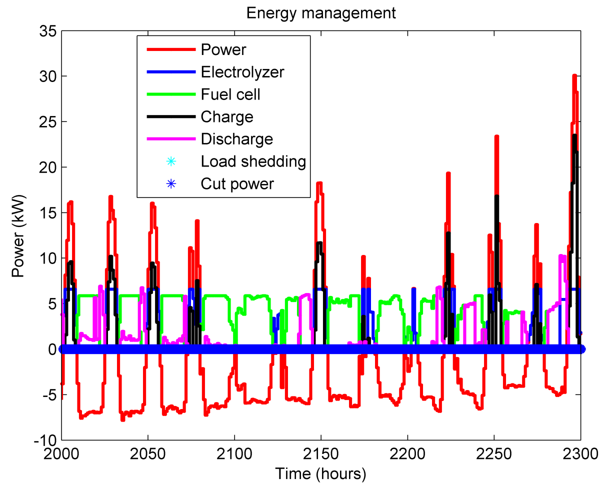

Figure 19: One-hour one-day rolling horizon scheduling simulation (2000 h-2300 h). The curve labelled 'Power' corresponds to the PV output minus the load.

5.9. *Influence of uncertainty*

As discussed earlier, uncertainty on forecasts of PV output and load can impact sizing results. To account for this uncertainty, the upper bound and lower bounds of estimated values are used. In the following, $\widetilde{P_{PV}(t)}$ and $\widetilde{P_{load}(t)}$ are the actual PV output and load values, and Er_{PV} and Er_{load} the error on PV output and load, respectively. The lower and upper bounds are then obtained with $\widetilde{P_{PV}(t)} = P_{PV}(t) \pm P_{PV}(t) \cdot Er_{PV}$ and $\widetilde{P_{load}(t)} = P_{load}(t) \pm P_{load}(t) \cdot Er_{load}$.

Two cases are defined. The worst case (the case where the difference between PV output and load is the largest) is when

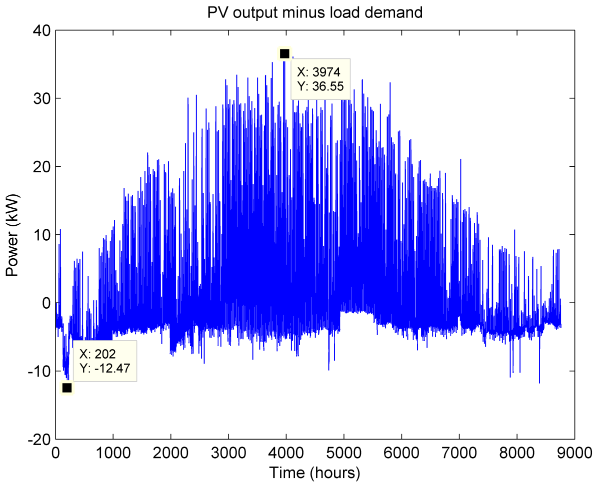

Figure 20: PV output minus load demand.

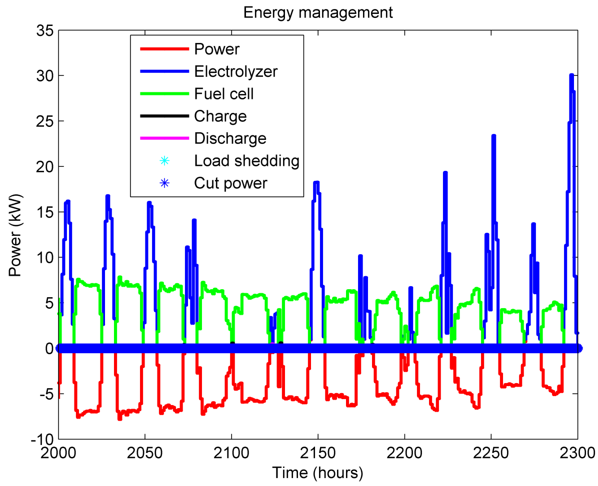

Figure 22: One-hour one-day rolling horizon scheduling simulation with the new sizing value of HSS (2000 h-2300 h). The curve labelled 'Power' corresponds to the PV output minus the load.

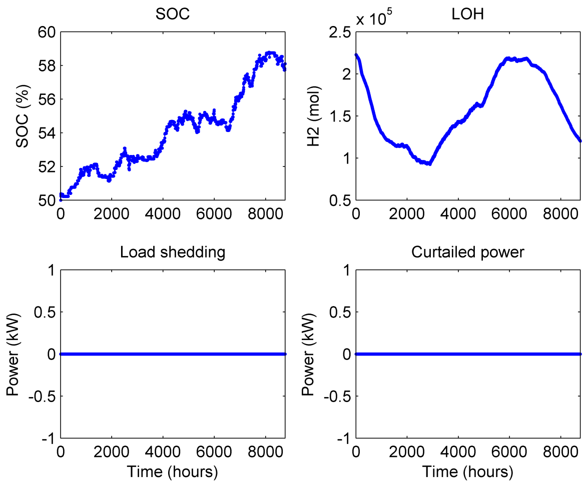

Figure 21: One-hour one-day rolling horizon scheduling simulation with the new sizing value of HSS.

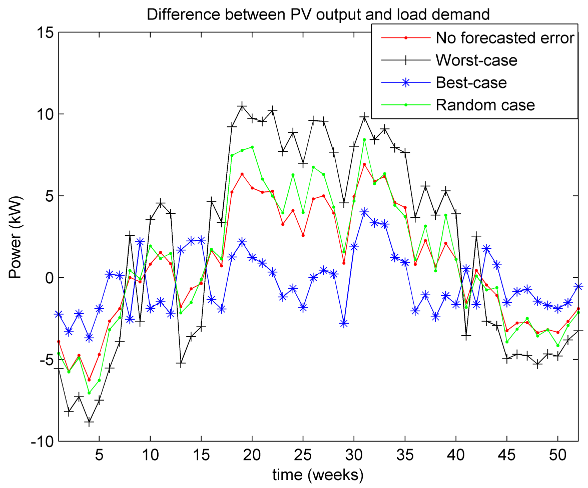

Figure 23: Difference between PV output and load demand in 4 cases.

PV output is equal to the upper bound value, and load is equal to the lower bound value; or when PV output is equal to the lower bound value, load is equal to the upper bound value. For the best case (the case where the difference between PV output and load is the lowest), the opposite is used.

Values for $\widetilde{P_{PV}(t)}$ minus $\widetilde{P_{load}(t)}$ are shown in Fig. 23. If the sizing results can satisfy the worst and best cases, then others cases can also be satisfying by the obtained sizing results. This means that the worst and best case data must be used to run the co-optimization method and obtain the sizing results. Table 5 shows the sizing results when $Er_{PV} = Er_{load} = 0.1$. For the worst-case, the HSS used frequently because it is cheaper than BSS. For the best case, the BSS is used frequently due to limitations of the HSS (minimum startup power), so more BSS capacity is needed.

6. Conclusion

In this paper, we present a methodology to determine the optimal sizing for a stand-alone microgrid. This methodology combines an EA for sizing and MILP for scheduling, and enables considering advanced energy management strategies, capable of anticipating decisions (especially with respect to storage), compared to classical rule-based approaches. Results show that the operation strategy, initial conditions, time resolution as well as uncertainty on input data influence the sizing of the components, and consequently the total cost of the microgrid. A comparison with a rule-based operation strategy is run, and sizing results show that co-optimization method performs better. A rolling-horizon simulation is used to adjust the sizing values due to the influence of input data time resolution. At last, forecasting errors are taken into account using a robust method, to further adjust sizing results. With the proposed method and complements, the proposed method can therefore be used for

Table 5: Sizing results considering uncertainty. The worst case is defined as the case where the difference between PV output and load is the largest, and the lowest for the best case.

Case	Total Cost [€]	C_{op} [€]	C_{cap} [€]	N_{PV}	P_{fc}^{max} [kW]	P_{el}^{max} [kW]	V_{H_2} [N.m^3]	C_{bat} [kWh]
Worst case	279270	1761.7	166960	50	8	8	11022	11
Best case	174400	1617.2	113450	50	6	6	5875	269

economically sizing a microgrid containing PV panels, a BSS and an HSS.

7. References

[1] N. Lidula, A. Rajapakse, Microgrids research: A review of experimental microgrids and test systems, Renewable and Sustainable Energy Reviews 15 (1) (2011) 186–202.

[2] N. Hatziargyriou, H. Asano, R. Iravani, C. Marnay, Microgrids, IEEE power and energy magazine 5 (4) (2007) 78–94.

[3] Y. A. Katsigiannis, P. S. Georgilakis, E. S. Karapidakis, Hybrid simulated annealing–tabu search method for optimal sizing of autonomous power systems with renewables, Sustainable Energy, IEEE Transactions on 3 (3) (2012) 330–338.

[4] G. Kyriakarakos, A. I. Dounis, S. Rozakis, K. G. Arvanitis, G. Papadakis, Polygeneration microgrids: a viable solution in remote areas for supplying power, potable water and hydrogen as transportation fuel, Applied Energy 88 (12) (2011) 4517–4526.

[5] Y. Wang, C. Chen, J. Wang, R. Baldick, Research on resilience of power systems under natural disasters-a review, IEEE Transactions on Power Systems 31 (2) (2016) 1604–1613.

[6] C. Abbey, D. Cornforth, N. Hatziargyriou, K. Hirose, A. Kwasinski, E. Kyriakides, G. Platt, L. Reyes, S. Suryanarayanan, Powering through the storm: microgrids operation for more efficient disaster recovery, IEEE power and energy magazine 12 (3) (2014) 67–76.

[7] A. A. Akhil, G. Huff, A. B. Currier, B. C. Kaun, D. M. Rastler, S. B. Chen, A. L. Cotter, D. T. Bradshaw, W. D. Gauntlett, Electricity storage handbook, Tech. rep., DOE/EPRI in collaboration with NRECA (2013).

[8] G. Kyriakarakos, D. D. Piromalis, K. G. Arvanitis, A. I. Dounis, G. Papadakis, On battery-less autonomous polygeneration microgrids: Investigation of the combined hybrid capacitors/hydrogen alternative, Energy Conversion and Management 91 (2015) 405–415.

[9] G. Cau, D. Cocco, M. Petrollese, S. K. Kær, C. Milan, Energy management strategy based on short-term generation scheduling for a renewable microgrid using a hydrogen storage system, Energy Conversion and Management 87 (2014) 820–831.

[10] J. Larminie, A. Dicks, M. S. McDonald, Fuel cell systems explained, Vol. 2, Wiley New York, 2003.

[11] S. G. Tesfahunegn, Fuel cell assisted photovoltaic power systems.

[12] T. Lajnef, S. Abid, A. Ammous, Modeling, control, and simulation of a solar hydrogen/fuel cell hybrid energy system for grid-connected applications, Advances in Power Electronics 2013.

[13] M. Uzunoglu, O. Onar, M. Alam, Modeling, control and simulation of a pv/fc/uc based hybrid power generation system for stand-alone applications, Renewable Energy 34 (3) (2009) 509–520.

[14] R. P. Menon, M. Paolone, F. Maréchal, Study of optimal design of polygeneration systems in optimal control strategies, Energy 55 (2013) 134–141.

[15] A. Maleki, F. Pourfayaz, Optimal sizing of autonomous hybrid photovoltaic/wind/battery power system with lpsp technology by using evolutionary algorithms, Solar Energy 115 (2015) 471–483.

[16] W. Zhou, C. Lou, Z. Li, L. Lu, H. Yang, Current status of research on optimum sizing of stand-alone hybrid solar–wind power generation systems, Applied Energy 87 (2) (2010) 380–389.

[17] D. Connolly, H. Lund, B. V. Mathiesen, M. Leahy, A review of computer tools for analysing the integration of renewable energy into various energy systems, Applied Energy 87 (4) (2010) 1059–1082.

[18] A. Maleki, A. Askarzadeh, Comparative study of artificial intelligence techniques for sizing of a hydrogen-based stand-alone photovoltaic/wind hybrid system, international journal of hydrogen energy 39 (19) (2014) 9973–9984.

[19] A. Fetanat, E. Khorasaninejad, Size optimization for hybrid photovoltaic–wind energy system using ant colony optimization for continuous domains based integer programming, Applied Soft Computing 31 (2015) 196–209.

[20] A. Maleki, A. Askarzadeh, Artificial bee swarm optimization for optimum sizing of a stand-alone pv/wt/fc hybrid system considering lpsp concept, Solar Energy 107 (2014) 227–235.

[21] A. Maleki, M. Ameri, F. Keynia, Scrutiny of multifarious particle swarm optimization for finding the optimal size of a pv/wind/battery hybrid system, Renewable Energy 80 (2015) 552–563.

[22] B. Zhao, X. Zhang, P. Li, K. Wang, M. Xue, C. Wang, Optimal sizing, operating strategy and operational experience of a stand-alone microgrid on dongfushan island, Applied Energy 113 (2014) 1656–1666.

[23] R. Atia, N. Yamada, Optimization of a pv-wind-diesel system using a hybrid genetic algorithm, in: Electrical Power and Energy Conference (EPEC), 2012 IEEE, IEEE, 2012, pp. 80–85.

[24] B. Bahmani-Firouzi, R. Azizipanah-Abarghooee, Optimal sizing of battery energy storage for micro-grid operation management using a new improved bat algorithm, International Journal of Electrical Power & Energy Systems 56 (2014) 42–54.

[25] C.-S. Karavas, G. Kyriakarakos, K. G. Arvanitis, G. Papadakis, A multi-agent decentralized energy management system based on distributed intelligence for the design and control of autonomous polygeneration microgrids, Energy Conversion and Management 103 (2015) 166–179.

[26] M. Marzband, M. Javadi, J. L. Domınguez-Garcıa, M. M. Moghaddam, Non-cooperative game theory based energy management systems for energy district in the retail market considering der uncertainties, IET Generation, Transmission & Distribution.

[27] M. Marzband, N. Parhizi, M. Savaghebi, J. M. Guerrero, Distributed smart decision-making for a multimicrogrid system based on a hierarchical interactive architecture, IEEE Transactions on Energy Conversion 31 (2) (2016) 637–648.

[28] M. Marzband, F. Azarinejadian, M. Savaghebi, J. M. Guerrero, An optimal energy management system for islanded microgrids based on multiperiod artificial bee colony combined with markov chain, IEEE SYSTEMS JOURNAL.

[29] M. Marzband, E. Yousefnejad, A. Sumper, J. L. Domínguez-García, Real time experimental implementation of optimum energy management system in standalone microgrid by using multi-layer ant colony optimization, International Journal of Electrical Power & Energy Systems 75 (2016) 265–274.

[30] M. Marzband, M. Ghadimi, A. Sumper, J. L. Domínguez-García, Experimental validation of a real-time energy management system using multi-period gravitational search algorithm for microgrids in islanded mode, Applied energy 128 (2014) 164–174.

[31] M. Marzband, N. Parhizi, J. Adabi, Optimal energy management for stand-alone microgrids based on multi-period imperialist competition algorithm considering uncertainties: experimental validation, International transactions on electrical energy systems.

[32] M. Marzband, A. Sumper, A. Ruiz-Álvarez, J. L. Domínguez-García, B. Tomoiagă, Experimental evaluation of a real time energy management system for stand-alone microgrids in day-ahead markets, Applied Energy 106 (2013) 365–376.

[33] P. Murty, Operation and control in power systems, BS Publications, 2011.

[34] R. Hemmati, H. Saboori, Short-term bulk energy storage system scheduling for load leveling in unit commitment: modeling, optimization, and sensitivity analysis, Journal of advanced research 7 (3) (2016) 360–372.

[35] K. P. Detroja, Optimal autonomous microgrid operation: A holistic view, Applied Energy 173 (2016) 320–330.

[36] L. Guo, W. Liu, J. Cai, B. Hong, C. Wang, A two-stage optimal planning and design method for combined cooling, heat and power microgrid

system, Energy Conversion and Management 74 (2013) 433 – 445.

[37] J. S. Kim, T. F. Edgar, Optimal scheduling of combined heat and power plants using mixed-integer nonlinear programming, Energy 77 (2014) 675–690.

[38] M. Marzband, A. Sumper, J. L. Domínguez-García, R. Gumara-Ferret, Experimental validation of a real time energy management system for microgrids in islanded mode using a local day-ahead electricity market and minlp, Energy Conversion and Management 76 (2013) 314–322.

[39] H. Daneshi, A. K. Srivastava, Security-constrained unit commitment with wind generation and compressed air energy storage, Generation, Transmission & Distribution, IET 6 (2) (2012) 167–175.

[40] R. Palma-Behnke, C. Benavides, F. Lanas, B. Severino, L. Reyes, J. Llanos, D. Sáez, A microgrid energy management system based on the rolling horizon strategy, Smart Grid, IEEE Transactions on 4 (2) (2013) 996–1006.

[41] S. Parhoudeh, A. Baziar, A. Mazareie, A. Kavousi-Fard, A novel stochastic framework based on fuzzy cloud theory for modeling uncertainty in the micro-grids, International Journal of Electrical Power & Energy Systems 80 (2016) 73–80.

[42] A. Zakariazadeh, S. Jadid, P. Siano, Smart microgrid energy and reserve scheduling with demand response using stochastic optimization, International Journal of Electrical Power & Energy Systems 63 (2014) 523–533.

[43] Y. Xiang, J. Liu, Y. Liu, Robust energy management of microgrid with uncertain renewable generation and load, IEEE Transactions on Smart Grid 7 (2) (2016) 1034–1043.

[44] E. Kuznetsova, Y.-F. Li, C. Ruiz, E. Zio, An integrated framework of agent-based modelling and robust optimization for microgrid energy management, Applied Energy 129 (2014) 70–88.

[45] A. Hussain, V.-H. Bui, H.-M. Kim, Robust optimization-based scheduling of multi-microgrids considering uncertainties, Energies 9 (4) (2016) 278.

[46] G. Liu, K. Tomsovic, Robust unit commitment considering uncertain demand response, Electric Power Systems Research 119 (2015) 126–137.

[47] F. Valencia, J. Collado, D. Sáez, L. G. Marín, Robust energy management system for a microgrid based on a fuzzy prediction interval model, IEEE Transactions on Smart Grid 7 (3) (2016) 1486–1494.

[48] R. Dufo-Lopez, J. L. Bernal-Agustín, J. Contreras, Optimization of control strategies for stand-alone renewable energy systems with hydrogen storage, Renewable energy 32 (7) (2007) 1102–1126.

[49] A. Khodaei, M. Shahidehpour, Microgrid-based co-optimization of generation and transmission planning in power systems, IEEE transactions on power systems 28 (2) (2013) 1582–1590.

[50] A. Khodaei, S. Bahramirad, M. Shahidehpour, Microgrid planning under uncertainty, IEEE Transactions on Power Systems 30 (5) (2015) 2417–2425.

[51] J. Zhang, K.-J. Li, M. Wang, W.-J. Lee, H. Gao, A bi-level program for the planning of an islanded microgrid including caes, in: Industry Applications Society Annual Meeting, 2015 IEEE, IEEE, 2015, pp. 1–8.

[52] L. Xu, X. Ruan, C. Mao, B. Zhang, Y. Luo, An improved optimal sizing method for wind-solar-battery hybrid power system, Sustainable Energy, IEEE Transactions on 4 (3) (2013) 774–785.

[53] P. Diéguez, A. Ursúa, P. Sanchis, C. Sopena, E. Guelbenzu, L. Gandía, Thermal performance of a commercial alkaline water electrolyzer: experimental study and mathematical modeling, international journal of hydrogen energy 33 (24) (2008) 7338–7354.

[54] Ø. Ulleberg, Modeling of advanced alkaline electrolyzers: a system simulation approach, International journal of hydrogen energy 28 (1) (2003) 21–33.

[55] F. Laurencelle, R. Chahine, J. Hamelin, K. Agbossou, M. Fournier, T. Bose, A. Laperriere, Characterization of a ballard mk5-e proton exchange membrane fuel cell stack, Fuel Cells 1 (1) (2001) 66–71.

[56] F. Garcia, C. Bordons, Optimal economic dispatch for renewable energy microgrids with hybrid storage using model predictive control, in: Industrial Electronics Society, IECON 2013-39th Annual Conference of the IEEE, IEEE, 2013, pp. 7932–7937.

[57] T. M. Hansen, R. Roche, S. Suryanarayanan, A. A. Maciejewski, H. J. Siegel, Heuristic optimization for an aggregator-based resource allocation in the smart grid, IEEE Transactions on Smart Grid 6 (4) (2015) 1785–1794. doi:10.1109/TSG.2015.2399359.

[58] R. Roche, S. Suryanarayanan, T. M. Hansen, S. Kiliccote, A. Miraoui, A multi-agent model and strategy for residential demand response coordination, in: PowerTech, 2015 IEEE Eindhoven, 2015, pp. 1–6. doi:10.1109/PTC.2015.7232268.

[59] G. Ferrari-Trecate, E. Gallestey, P. Letizia, M. Spedicato, M. Morari, M. Antoine, Modeling and control of co-generation power plants: a hybrid system approach, IEEE Transactions on Control Systems Technology 12 (5) (2004) 694–705.

[60] B. Colson, P. Marcotte, G. Savard, An overview of bilevel optimization, Annals of operations research 153 (1) (2007) 235–256.

[61] J. Lagorse, D. Paire, A. Miraoui, Sizing optimization of a stand-alone street lighting system powered by a hybrid system using fuel cell, {PV} and battery, Renewable Energy 34 (3) (2009) 683 – 691.

[62] M. Castañeda, A. Cano, F. Jurado, H. Sanchez, L. M. Fernandez, Sizing optimization, dynamic modeling and energy management strategies of a stand-alone pv/hydrogen/battery-based hybrid system, International journal of hydrogen energy 38 (10) (2013) 3830–3845.